Variations around disordered close packing

2005 J. Phys.: Condens. Matter 17 S2361

(http://iopscience.iop.org/0953-8984/17/24/001)

INSTITUTE OF PHYSICS PUBLISHING JOURNAL OF PHYSICS: CONDENSED MATTER

J. Phys.: Condens. Matter **17** (2005) S2361–S2390 doi:10.1088/0953-8984/17/24/001

Variations around disordered close packing

T Aste

Department of Applied Mathematics, RSPhysSE, Australian National University, 0200, Australia

Received 4 April 2005
Published 3 June 2005
Online at stacks.iop.org/JPhysCM/17/S2361

Abstract

The most suitable paradigms and tools for investigating the structure of granular packings are reviewed and discussed in the light of some recent empirical results. I examine the 'typical' local configurations, their relative occurrences, their correlations, their organization and the resulting overall hierarchical structure. The analysis of very large samples of monosized spheres packed in a disorderly fashion, with packing fractions ρ ranging from 0.58 to 0.64, demonstrates the existence of clear relations between the geometrical structure and the packing density ρ. It is observed that the local Delaunay and Voronoï volumes have distributions which decay exponentially at large volumes, and have characteristic coefficients proportional to ρ. The average number of contacts per sphere grows linearly with ρ. The topological density increases with ρ and it is larger than the corresponding one for lattice sphere packing. The heights and the shapes of the peaks in the radial distribution function also depend on ρ. Moreover, the study of several other quantities, such as the dihedral angle distribution, the fractions of four-, five-and six-membered rings and the shape of the Voronoï cells, shows that the local organization has characteristic patterns which depend on the packing density. All the empirical evidence excludes the possibility of the presence of any crystalline order, even at the minimal correlation length (one bead diameter). Moreover, icosahedral order and other close packed configurations have no statistical significance, excluding therefore the possibility that geometrical frustration could play any significant role in the formation of such amorphous structures. On the other hand, the analysis of the local geometrical 'caging' discloses that, at densities above 0.601, the system can no longer explore the phase space by means of local moves only and it becomes trapped either in the basin of attractions of inherent states, with limiting densities in the range 0.61–0.64, or in the crystalline branch.

(Some figures in this article are in colour only in the electronic version)

1. Introduction

In order to fully classify the state of a disordered system, such as a granular packing at rest, complete information about the exact position, orientation and shape of each grain is—in principle—needed. However, part of such information is redundant or irrelevant and several degenerate states with different microscopic realizations can share the same macroscopic properties. Identifying which are the accessible configurations at local level and understanding which are the possible combinations of such local configurations for generating the global packing is of fundamental importance and it is the necessary starting point for any further understanding of these systems.

Until now the empirical investigation of the geometrical structure of these systems has been limited by the very low availability of accurate experimental data. Following on from the seminal works of Bernal, Mason and Scott [1–3], only very recently has the use of tomography allowed one to ‘see’ three-dimensional structures and explore their geometry from the grain level up to the whole packing.

To our knowledge, the first work which uses tomographic techniques devoted to the investigation of granular packing was a paper by Seidler *et al* appeared in the year 2000 [4]. Two other works, by Sederman *et al* [5] and Richard *et al* [6], followed respectively in 2001 and 2003. Confocal microscopy techniques have also been used to reconstruct 3D images of a dense packing emulsion of oil droplets [7] and to count contacts in glass beads [8]. However, all these works concern rather small samples and focus on particular topics. In this paper we refer to an empirical investigation by means of x-ray computed tomography on very large samples of monosized spheres packed in a disorderly fashion with packing densities ranging from 0.58 to 0.64. (Recall that the density is defined as the fraction of the volume occupied by the balls divided by the total volume of the region of space considered.) The empirical results were presented in a preliminary form in [9] and in a more complete form in [10]. These studies are the largest and the most accurate empirical analysis of disordered packings at the grain scale ever performed. A detailed description of the experimental methodology and apparatus is reported in the papers [9, 10]. Let us recall here that we analysed six samples of monosized acrylic spheres all in a cylindrical container with an inner diameter of 55 mm with rough walls, filled with equal sized beads to a height of $\sim$75 mm. In order to verify possible effects due to gravity and sizes we used two kinds of acrylic spheres, with diameters $d = 1.00$ mm and $d = 1.59$ mm, with polydispersities within 0.05 mm. The smaller spheres were used to prepare two samples at densities 0.586 and 0.619 containing respectively about 103 000 and 143 000 spheres (referred as samples A and C hereafter), whereas with the larger spheres we prepared four samples at densities 0.596, 0.626, 0.630 and 0.64 (samples B, D, E and F) each containing about 35 000 beads. An x-ray computed tomography apparatus (see [11]) was used to image the samples. The two large samples (A, C) were analysed by acquiring data sets of 2000^3 voxels with a spatial resolution 0.03 mm, whereas for the other four samples (B, D, E and F) we acquired data sets of 1000^3 voxels with a spatial resolution of 0.06 mm. The positions of the centres of each of the sphere were retrieved (with a sub-voxel precision) by a convolution method applied to the segmented [12] data sets (see [9, 10] for further details). The geometrical investigation of the packing structure was performed over a central region (**G**) at four sphere diameters away from the sample boundaries. (Note that spheres outside **G** are considered when computing the neighbouring environment of spheres in **G**.) The two large samples have about 56 000 and 92 000 spheres in **G**, whereas the four smaller ones have about 16 000 spheres in this region.

In the present paper I review several investigation techniques for studying disordered sphere packings and I discuss the application of such techniques to the analysis of samples A–F [9, 10, 13, 14]. The paper is organized as follows.

In section 2, the existence of four distinct density regions each associated with specific geometrical and behavioural properties is discussed.

In section 3, local volume fluctuations in sphere packings at different densities are analysed.

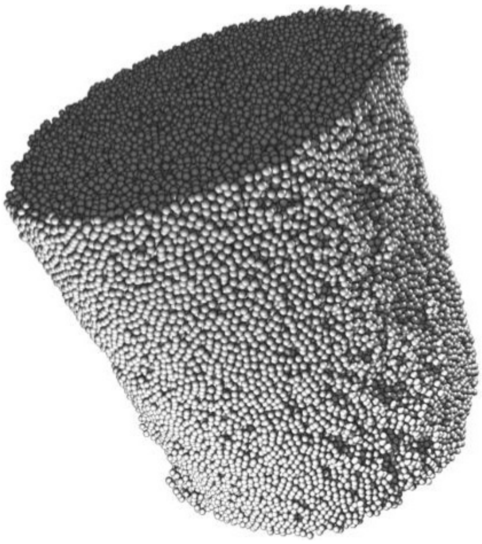

Figure 1. Volume rendering of an ~150 000-sphere packing in a cylindrical container.

The average number of spheres in contact with a given sphere and their distribution in the packings are discussed in section 4.

In section 5, stability, rigidity and jamming properties in these systems are reviewed in the light of the empirical findings.

The structure of the contact network beyond first neighbours is analysed in section 6.

In section 7 the structural properties emerging from the radial distribution function are reviewed in detail.

The typical local orientational symmetry and its relation with known configurations is discussed in section 8.

Techniques for analysing local geometrical correlations between more than two particles are discussed and applied in section 9.

Finally, the implications that the observed geometrical structure has for the system dynamical evolution are studied in section 10.

The conclusions in section 11 summarize the main results and perspectives.

In order to help readers and allow them to skip parts or concentrate on certain topics, each section of the paper has been designed to be self-contained, with cross-references to other sections where necessary.

2. Four packing density regions

When equal balls are packed in a container under gravity they occupy a fraction between 55% and 74% of the volume depending on the way the packing is formed and organized at grain level. The densest packing is achieved by an ordered stack of balls in parallel hexagonal layers forming the so-called Barlow packings at density $\rho = \pi/\sqrt{18} \sim 0.74$ [15, 16]. Volume fractions between 0.74 and 0.64 can be produced by introducing a certain amount of disorder (vacancies, crystalline defects, polycrystalline regions etc) starting from an ordered Barlow packing. On the other hand, if the balls are poured into the container they arrange themselves in a disorderly fashion and the packing results typically in densities between 0.61 and 0.62 (depending on the kinds of balls, the shape of the container, the speed and height from which they are poured). Larger densities up to around 0.63 can be reached by gently tapping the

Table 1. Sample density and the intervals of variations (±) within each sample; number of spheres in the sample (N); number of spheres in the central region (N_G); estimated average number of neighbours in contact (n_c), average number of neighbours at a given radial distance ($n_t(r)$ with $r = 1, 1.02, 1.05, 1.1$ diameters). Standard deviation (ξ) calculated from the probability distribution for radial distances smaller than d between pairs of sphere centres.

	Density	N	N_G	n_c	$n_t(1)$	$n_t(1.02)$	$n_t(1.05)$	$n_t(1.1)$	ξ/d
A	0.586 ± 0.005	102 897	54 719	**5.81** $\pm$ 0.3	3.0	5.5	6.7	7.5	0.014
B	0.596 ± 0.006	34 016	15 013	**5.91** $\pm$ 0.2	2.9	5.9	6.8	7.7	0.011
C	0.619 ± 0.005	142 919	91 984	**6.77** $\pm$ 0.2	3.5	6.4	7.5	8.4	0.013
D	0.626 ± 0.008	35 511	15 725	**6.78** $\pm$ 0.2	3.3	6.0	7.5	8.4	0.017
E	0.630 ± 0.01	35 881	15 852	**6.95** $\pm$ 0.2	3.4	6.3	7.6	8.6	0.016
F	0.640 ± 0.005	36 461	16 247	**6.97** $\pm$ 0.2	3.3	6.9	7.9	8.9	0.011

container, whereas to achieve the so-called random close packing limit at approximately 0.64 it seems necessary to add a small compression from above while tapping (see [9, 10]). Controlled vertical taping of a stack of grains in a tube has been used in several works [17–20] to induce progressive densification in the system and it has been noted that a steady plateau at densities comparable to the density obtained by simply pouring the grains can be obtained in a reproducible way by tuning the induced maximal acceleration to between 1 and 6 times the gravitational one [20]. All the available data in the literature indicate that densities above 0.64 cannot be achieved without partial crystallization. Densities below 0.60 can only be achieved by special treatments of the system. In particular in [17–20] loose packing densities in the range 0.577–0.583 were obtained by flowing dry nitrogen through the container from the bottom. Loose packings at densities 0.58–0.59 can be also produced by using a special technique which has been known for thousands of years and it was used by the sellers of dry grains to increase profits by improving of about 10% the volume occupied by the granular packing. This technique consists in pouring the spheres into the container with a stick inserted inside and slowly removing the stick after pouring. Intermediate densities (0.59–0.61) can be produced by shaking these loose structures. However these intermediate values are not stable under shaking and any action tends to densify the system up to the region between 0.61 and 0.63 within which the density can be increased or decreased in a reversible way depending on the kind of action performed on the system [17–20]. The lowest achievable limit for a stable packing is 0.555 (which coincides with the dilatancy onset) but such a limit can only be reached by reducing the effect of gravity [21].

In [9, 10] we observed that typically the density is not homogeneously distributed in different parts of the samples. This is also discussed by several other works (see for instance [19, 20]). In the samples A–F the densities are smaller than the average in a region close to the cylinder central axis; the density increases moving forward from the centre, then it saturates to rather homogeneous values up to a distance of a few (2–3) sphere diameters from the boundary. Rather inhomogeneous densities are also observed in the vertical direction, but in this case we find different behaviours depending on the sample preparation. However, we verify that in all the sample sub-regions the densities stay in a rather narrow range (within ±0.01) around the average densities. More importantly we verify that none of the computed structural properties change significantly in their behaviours and characteristics with the part of sample analysed. In the second column of table 1, the average density values for samples A–F and their intervals of variation are reported.

Summarizing, from all the empirical investigations available in the literature we can deduce that there are four rather well defined density regions: **0.55–0.58** where packings can be created only if the effect of gravity is reduced; **0.58–0.61** where packings can be generated but they are unstable under tapping; **0.61–0.64** where reversible structures can be created by pouring grains into the container and tapping for sufficiently long times (however it is not completely established whether the region 0.63–0.64 can be reached only by tapping or whether some combined compression must be added); **0.64–0.74** where crystallization is present. The challenge is now to establish whether there is a unique 'smooth' bijective relation between the sample density and its packing structure and whether such a structure is independent of the preparation procedure. The results reported in [9, 10] and the one discussed in the present paper are rather encouraging, showing that all the structural properties have a rather simple and monotonic dependence on the density. This suggests that the static state of the system can be uniquely identified by its density which is therefore the most relevant control parameter in monosized sphere packings. A very relevant point is now to understand which is the typical combination of local configurations which generate a packing at a given density and why the realizations of the system are naturally possible only within a restricted range of densities.

3. Local volume fluctuations

In this section we discuss how space is repartitioned around the spheres. Indeed, in a given packing some local configurations are closer and others are looser and the whole packing is made by gluing these local configurations together in a disordered way which is compatible with mechanical stability, geometrical constraints and global density. The first problem to address is how to divide the whole space into parts associated with the local environment around each sphere. In this respect, there are two natural ways to subdivide space into smaller portions. The first is the *Delaunay* decomposition, by which space is divided into simplexes with vertices on the centres of the neighbouring spheres chosen in such a way that no other spheres in the packing have centres within the circumsphere of the Delaunay simplex. The second possibility is the *Voronoï* decomposition which associates with each sphere a polyhedral cell delimiting the portion of space closest to the sphere centre with respect to any other centre in the packing. These two decompositions are geometrically dual and can be combined in several ways leading to other classes of decompositions (Q-systems and stars) [16].

The study of how space is shared among the packed spheres is essential for understanding how efficiently the spheres are arranged locally. Moreover, from a theoretical perspective it has been argued by Edwards [22, 23] that granular systems under tapping dynamics in the stationary regime can be described in terms of a Gibbs-like equilibrium thermodynamical approach where the constraint over the system energy is replaced with a constraint on the volume. This implies that the probability of a state with volume V must follow a Boltzmann distribution: $P(V) \propto \exp(-V/(\lambda X))$, with X the 'compactivity' (an intensive thermodynamic variable analogous to the temperature) and λ a constant analogous to the Boltzmann one. In a recent paper [24] Edwards and co-authors showed that the local volume fluctuations in a dense packing of emulsion oil droplets do indeed follow quite well an exponential distribution with coefficient $\lambda X = 119$.

In [13] we subdivided the samples into their Delaunay simplexes and calculated the volume of each simplex. We observed that such volumes follow distributions which, at large volumes, are well described by the exponential behaviour $P(v) \propto \exp(-\beta v/d^3)$ (see figure 2). We found that the coefficients β grow with the density ranging between $\sim$44 at $\rho = 0.586$ (sample A) and $\beta \sim 73$ at $\rho = 0.64$ (sample F) (see figure 2(*b*)). The plot of β^{-1} versus ρ reveals an impressive linear behaviour. Very similar behaviours and coefficients were also found for the distributions of the Delaunay 'free' volumes (the part of the Delaunay simplex not occupied by the balls).

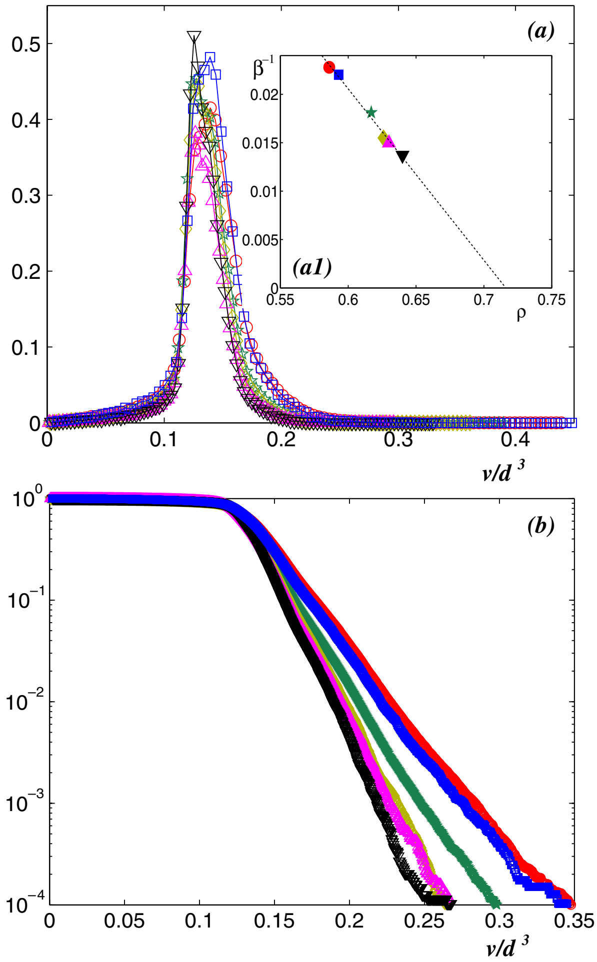

Figure 2. (a) Distribution of Delaunay volumes in **G**. ($a1$) Best fit values for the coefficients β^{-1} versus the inverse of the sample density ρ^{-1}. (b) The inverse normalized cumulants show tails that decrease linearly on a semilogarithmic scale: $p(V) \sim \exp(-\beta V/d^3)$ (best fits: $\beta = 43.9;\ 45.4;\ 55.2;\ 64.6;\ 66.8;\ 72.9$).

As discussed at the beginning of this section there are several ways to divide the whole space into sub-parts and the Voronoï construction is one of the most commonly used partitions. In order to verify the effect of the partition criteria on the local volume distributions, we calculated the volume distribution of the Voronoï cells constructed around the centres of each sphere in the samples. Figure 3 shows the distributions ($P(v)$) of these local volumes in **G** for the six samples. In this case we observe bell-shaped distributions with a clear skewness and fatter tails on the right-hand side. In figures 3(b), ($b1$) we show that the tails of such distributions can be interpolated with an exponential trend: $P(v) \propto \exp(-\beta' v/d^3)$ [13]. However, such a linear trend is less neat than in the Delaunay case and the coefficients β' are about 20% lower than the coefficients calculated from the Delaunay simplex decomposition. Such differences in the behaviours and the values of the coefficients pose a serious question as regards which kind of volume partition is more appropriate for the estimation of such quantities.

From a theoretical point of view, we can consider the whole system as an ensemble of local independent cells which freely exchange volume among themselves under the constraint that the sum over all the volumes must be a constant which characterizes the state of the system. If we assume that: (1) cells are undistinguishable (ignore their shapes); (2) there are no correlations among cells; (3) the geometrical constraints on the packing (stability, kissing

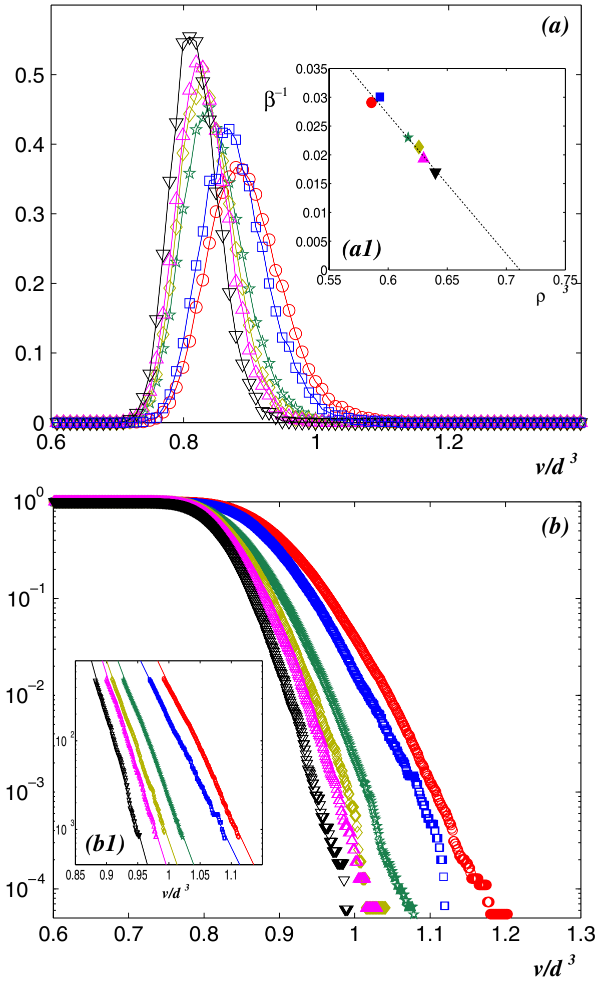

Figure 3. (a) Distribution of Voronoï volumes in **G** for the six samples. ($a1$) Best fit values for the coefficients β^{-1} versus the inverse of the sample density ρ^{-1}. (b) The inverse normalized cumulants show tails that decrease rather linearly on a semilogarithmic scale. ($b1$) Detail of the region where the fit with $p(V) \sim \exp(-\beta' V/d^3)$ has been performed (best fit values: $\beta' = 34.3$; 33.2; 43.5; 51.7; 58.9).

number etc) have no relevance, then the probability of finding a cell with a volume v must be simply given by $P(v) \propto \exp(-\beta v/d^3)$, with $\beta = d^3/\langle v\rangle$. Indeed, the above assumptions reduce the problem to the one-dimensional partitioning into several parts of a segment of size V and the probability distribution of the cell sizes can be calculated exactly. However, this simple argument predicts coefficients which are not satisfactory: we obtain $\beta \simeq 36\rho/\pi$ for the Delaunay partition and $\beta = 6\rho/\pi$ for the Voronoï partition, giving values for the coefficients which are an order of magnitude lower than the empirical coefficients. On the other hand, it is also evident from the figures 2 and 3 that these distributions are not pure exponentials. Further theoretical investigations are needed the explain such behaviours.

4. Number of spheres in contact

The average number of spheres in contact with a given sphere is probably the most commonly investigated parameter in the literature on granular packings [1–5, 8, 16, 25–29]. Indeed, this is a very simple topological quantity which gives important information about the local configurations and the packing stability and determines the cohesion of the material when liquid capillary bridges between particles are present. Moreover, historically this was the first topological quantity investigated in these systems [1, 2, 25]. Unfortunately, although simple in its definition, such a number is unavoidably an ill-defined quantity. Indeed, from a geometrical perspective, the information about the positions and eventually the sizes of all spheres is not sufficient to determine such a number: two spheres can be arbitrarily close but not touching. In the literature several physical methods have been used [1, 2, 8, 25], but they encounter problems all essentially associated with the uncertainty in the correct threshold distance which must be used to distinguish between 'touching' and non-touching spheres. In an early experiment [25] Smith poured lead shots into a beaker and then filled the beaker with a solution of acetic acid. The acid was then drained but a small ring of liquid was retained by capillarity at each contact point. After a few hours, white circular deposits at the contact positions were visible on the shots. The counting of the number of such marks on each shot led Smith to conclude that the number of contacts increases with the density and it is in the range between 6.9 and 9.14 for five samples with densities from 0.553 to 0.641. However, this early experiment is now considered not completely reliable because capillary necks of acid can also form between near but non-touching spheres and because the density 0.553 appears to be too small for a stable packing of monosized spheres under gravity (see section 2). A more precise but similar experiment was performed by Bernal and Mason about 30 years later [1]. In this experiment they used ball bearings compressed with a rubber band making a packing with density 0.62. The number of contacts was calculated by counting the number of marks left on the balls by a black japan paint after drainage. Unlike Smith, they distinguish between touching balls and 'nearly touching' balls, reporting an average number of touching spheres equal to 6.4 over an average number of 8.4 total marks. They estimated that with this method nearly touching balls are registered up to a distance 5% greater that the ball diameter. The same method, applied to a less dense packing with $\rho = 0.6$ (obtained by slowly rolling the balls in the container), gave 5.5 for the average number of touching spheres and 7.1 on adding the 'nearly touching' balls. In another experiment, a different method was adopted by Scott [2], who poured molten paraffin wax into a heated container filled with the balls packed at $\rho = 0.63$ and allowed the set-up to cool. In this way, after a great effort, he managed to calculate the Cartesian coordinates of a central cluster of about 1000 balls with a remarkable precision of less than 1% of their diameters. From these centre positions he computed an average number of 9.3 spheres within 1.1 diameters from the centres of the test spheres. However, a re-analysis of the same data [3] led Mason to conclude that there are about five touching spheres and a total of nearly seven neighbours within 1.02 diameters. (Later in this paper we will re-discuss this estimation in the light of a new method which yields a value around 7 for the number of spheres in contact.) Surprisingly, after this remarkable experiment by Scott, no further empirical investigations were performed until very recently when new techniques (confocal microscopy and x-ray microtomography) allowed visualization of the inside of the packing structures. In 2000, Seidler *et al* performed the first x-ray microtomography experiment on a monodisperse packing of glass spheres at density $\rho = 0.61$. They estimated the sphere centres with a precision of 1% diameters and calculated that there are an average of 8.3 neighbouring spheres within 1.06 diameters. In a recent experiment [8], the number of liquid bridges between glass beads in packings at density 0.62 were measured by zooming with an optical microscope. It was estimated that within a radial distance of $1.05d$, the number of neighbouring spheres must stay within the range 6 ± 1.5.

In the present paper we discuss the results reported in [9, 10] where the number of spheres in contact and the distribution were calculated with great accuracy for the six samples A–F with densities ranging between 0.578 and 0.64. Table 1 reports the values of the average numbers of neighbours (n_t) computed in **G** at the four different radial distances: $r = d$, $1.02d$, $1.05d$

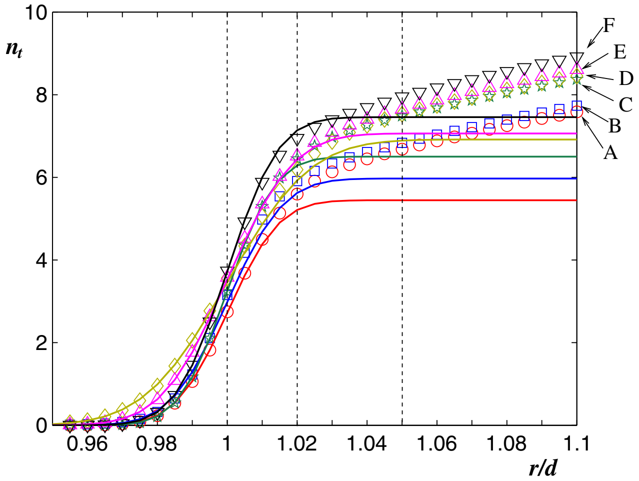

Figure 4. (symbols) Behaviour for the average number of sphere centres within a radial distance r. (lines) Error function normalized by best fitting the agreement with the data in the region $r < d$. The averages are d and the standard deviations (ξ) are calculated from the probability distribution for radial distances smaller than d between pairs of sphere centres. The renormalized error function fits well to the data for $r < d$. After this value, near neighbours not in contact start to contribute to $n_t(r)$ and the two behaviours split.

and $1.1d$. As one can see, this number increases with the radial distance and, across the six samples, n_t ranges between 3 and 8.9 depending on the threshold distance and sample density. A more precise estimate for the actual number of spheres in contact can be inferred from the behaviour of $n_t(r)$ (shown in figure 4 as a function of the radial distance up to $r = 1.1d$). From figure 4 one can note that above $r = 0.98d$ the number of neighbours grows very steeply up to a 'knee' at about $1.02d$, where a slower growth takes over. Such a steep growth in the number of neighbours can only be an effect of the spread in the statistical distribution of the distances between spheres in contact which is due to the polydispersity and the uncertainty in the positions of the sphere centres. Indeed, in the ideal case where all the exact positions of closely packed, identical, perfect spheres are known, one would expect $n_t(r)$ to have a discontinuity at $r = d$ (from zero to the number of neighbours in contact n_c) followed by some kind of growth for $r > d$. For real, polydisperse, non-perfect, spheroidal grains, the distance between elements in contact is not a fixed value but instead it is normally distributed. As a consequence, one expects the discontinuity at $r = d$ to enlarge into a complementary error function. Such an error function must be added to the contribution from the 'nearly touching' spheres which is expected to become sizable from $r > d$. We therefore expect to find an error function behaviour up to $r \sim d$ and then a combined contribution from the error function and some growing law describing the cumulated number of non-touching neighbours within the distance r. Indeed, we verify that the behaviour of $n_t(r)$ for $r \leqslant d$ is very well described by a complementary error function normalized to n_c:

$$n_t(r)^{\text{fit}} = n_c \frac{1}{\sqrt{2\pi\xi^2}} \int_{-\infty}^{r} \exp\left(-\frac{(x-d)^2}{2\xi^2}\right) \mathrm{d}x. \tag{1}$$

The value of the mean d is the average sphere diameter which was estimated: $d = 25.00$ voxels (samples B, D, E, F) and $d = 30.81$ voxels (samples A, C) [9, 10]. On the other hand, the variance ξ can be directly calculated from the data by computing the second moments $\langle (r-d)^2 \rangle$ for the radial distances between spheres calculated over half the distribution in the

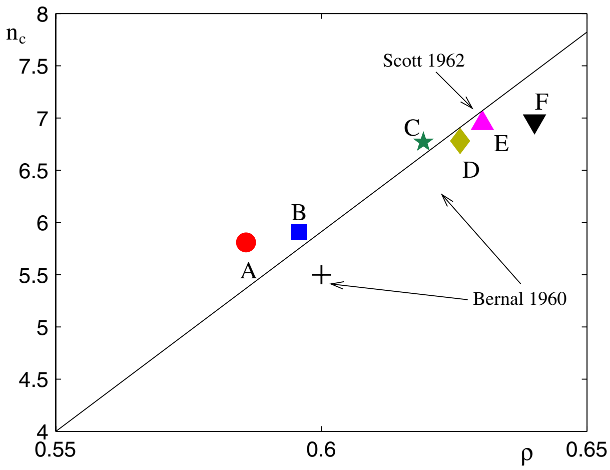

Figure 5. Number of neighbours in contact versus sample density. The filled symbols correspond to the samples investigated in the present work. The two symbols '+' show the values from [1] whereas the '×' shows that from [2, 3]. The line is the best fitting linear trend constrained to pass through $n_c = 4$ at $\rho = 0.55$.

region $r < d$:

$$\xi = 2\sqrt{\frac{\sum_{i,j}(r_{i,j} - d)^2 H(d - r_{i,j})}{\sum_{i,j} H(d - r_{i,j})}} \tag{2}$$

with i, j indices labelling the sphere centres; the symbol $r_{i,j}$ indicating the distances between the centres of spheres i and j; and $H(d - r_{i,j})$ the step function which returns 1 if $r_{i,j} < d$ and 0 if $r_{i,j} \geqslant d$. From equation (2) we retrieve variances ξ between $0.011d$ and $0.017d$ (all the values are reported in table 1). These values are consistent with the bead polydispersity and are significantly larger than the estimated uncertainty on the sphere centres. The only free parameter left in equation (1) is the value of n_c which can now be computed by best fitting the agreement between the data for $n_t(r)$ and the function $n_c^{\mathrm{fit}}(r)$ in the region $r < d$. In figure 4 it is shown that the function $n_c^{\mathrm{fit}}(r)$ fits well to the data for $r < d$ by using the values of n_c given in table 1. At larger distances $r > d$, near neighbours not in contact start to contribute to $n_t(r)$ and the two behaviours split. We estimate that in the six samples A–F there are on average between 5.81 and 6.97 spheres in contact (see table 1). These numbers fall in the range of the values for n_c reported in the literature based on some of the previous experimental observations (Bernal reports $n_c = 5.5$ at $\rho = 0.6$ and $n_c = 6.4$ at $\rho = 0.62$ [1], whereas from the data given by Scott we have $n_c = 7$ at $\rho = 0.63$ [2]). (Note that this last datum has been recalculated from the original data by applying the deconvolution method described above.)

In figure 5 the values of n_c versus density for the samples A–F are reported together with those from Bernal and Scott. As one can see, they all result in a rather good agreement. Such an agreement between these different data is remarkable considering the different experimental set-ups, the different preparations of the samples, the different criteria for identifying and counting spheres in contact and the different polydispersities of the spheres. As one can see from figure 5, they all show a clear and consistent increasing behaviour with the density. A similar increasing trend was also found in simulated packings [30, 31].

This dependence on the packing density has important theoretical implications which are discussed in the next section. But, before concluding this part, let me introduce a simple

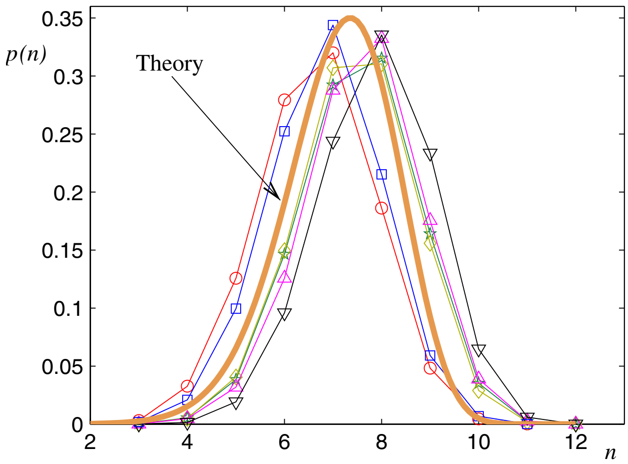

Figure 6. Distribution of the number of near neighbours at radial distances within 1.05 sphere diameters. The thick line is the theoretical behaviour predicted by a free-volume-like local theory (equation (4)) with $n^* = 12.99$.

theoretical argument to calculate the distribution of the number of neighbours around each sphere. Let us consider a local configuration composed of one sphere and n touching neighbours. First, let us compute the degrees of freedom of such a system in terms of the volume which can be explored in their configurational space. In particular, each one of the n surrounding spheres can span a solid angle of 4π but the non-overlapping condition implies that spheres cannot stay arbitrarily closed. It is indeed known that only 12 equal spheres can stay touching a central sphere (the kissing number [16]). However, the solid angle occupied by a sphere touching the central sphere is $4\pi/n_0$ with $n_0 = 4/(2-\sqrt{3}) = 14.928, \ldots$, which means that it occupies less than $1/14$ th of the total solid angle. This was the source for a famous discussion between Isaac Newton and David Gregory in 1694. Newton correctly believed that no more than 12 spheres can be packed touching a central sphere but Gregory thought that there might be a way to put 13. Indeed, there is a lot of available free space when 12 spheres are packed around a central one but not enough to accommodate 13. To calculate the free solid angle per sphere, we can therefore assume that each touching sphere occupies an 'effective' portion $4\pi/n^*$ of the total solid angle with n^* a number smaller than 13. For a configuration of n spheres around a central sphere we have consequently that the portion of solid angle, in which the particles can move freely is $4\pi - n4\pi/n^*$. From a different perspective this system can be viewed as a 'gas' of n particles in a box of volume $4\pi - n4\pi/n^*$ $(n^* < 13)$. The integration over the angular degrees of freedom of the n touching spheres gives a partition function of such a 'gas' which can be approximated as

$$Z_n = \left(4\pi - 4\pi\frac{n}{n^*}\right)^n \tag{3}$$

(where we used a free-volume kind of approximation [32]). In such a system the probability of a state with n touching neighbours must be

$$p(n) = \frac{(4\pi - 4\pi\frac{n}{n^*})^n}{\sum_n Z_n}. \tag{4}$$

In figure 6 the distributions of the number of near neighbours per sphere (within a distance $1.05d$) are reported for the six samples. As one can see, the behaviour predicted by equation (4) mimics well the empirical distributions using $n^* = 12.99$. This seems to indicate that the packing configurations form—in an almost unconstrained way—by maximizing local rotational degrees of freedom.

5. Stability, rigidity and jamming

In a stack of grains at mechanical equilibrium, Newton's equations for the balance of the force and torque acting on each grain must be satisfied. Lagrange and Maxwell [33, 34] were the first to note that in such systems, to achieve stability, the number of degrees of freedom must balance the number of constraints. If we consider a packing of N perfect, smooth spheres, a simple counting (known as Maxwell counting) gives $3N$ degrees of freedom (translational modes) and $n_c N/2$ constraints (one normal force per contact, n_c contacts on average and each contact shared by two spheres). In this case, the balance between freedom and constraints implies that n_c must be equal to 6 [35, 36]. On the other hand, real grains (for instance the acrylic beads in samples A–F) have unavoidably rotational modes and therefore the degrees of freedom number $6N$ (translational and rotational modes). Moreover some friction is always present; therefore tangential forces must also be considered yielding $3n_c N/2$ constraints on the contacts (three components of the force per contact, n_c contacts on average and each contact shared by two spheres). In this case the counting gives $n_c = 4$. This counting is rather encouraging: a very simple argument gives values for n_c which are close to the one observed experimentally. However, it must be noted that this condition for n_c is neither sufficient nor necessary [37–39]. Indeed, there can be local configurations which contribute to n_c but do not contribute to the whole system rigidity. (There are, for instance, the 'rattling' grains which can be removed from the system without affecting its stability.) On the other hand, there are local arrangements which satisfy the counting rule on n_c but nevertheless are not rigid [37, 38].

In recent years there have been a large number of theoretical approaches which consider real, disordered, granular packings to be isostatic (free of self-induced stresses) [35, 40]. The advantage is that in a system at the isostatic equilibrium, the intergranular forces are uniquely determined by the balance of force and torque alone. In contrast, an overconstrained structure can generate self-stress and the deformation of individual grains becomes relevant. In real granular materials (or in bead packings) friction and rotational degrees of freedom are unavoidable; therefore the Maxwell counting implies that isostatic configurations must have the average connectivity $n_c = 4$. Unfortunately, such a value is rather small in comparison with all the available empirical estimations. Moreover, all the experimental observations conclude that n_c increases with the packing density, excluding therefore the possibility of fixing n_c at 4 for all stable packings.

However, in related studies on the rigidity in network glasses [39, 41] it has been observed that there can exist two phase transitions associated with the increase of connectivity in a network: a *rigidity percolation* and a *stress percolation*, and between these two thresholds an *intermediate phase* which is rigid but unstressed. The *rigidity percolation* occurs at the threshold predicted by the Maxwell counting ($n_c = 4$) and it resembles a second-order transition. Whereas the *stress percolation* transition occurs at a higher value of n_c, it is much sharper and it could be a first-order transition [41]. This suggests that granular packings might be in a *marginal state* between the rigidity and the stress percolation thresholds. In such an isostatic unstressed state, the system has zero elastic moduli (in the thermodynamic limit) [39, 41]; it is therefore marginally rigid and it can be seen as in an intermediate state, between fluid and solid [42]. An extrapolation from the experimental data for n_c reported in figure 5 suggests that a grain connectivity equal to 4 could be reached by the system at the density $\rho = 0.55$. This would place the rigidity percolation threshold at the loose packing limit.

Another alternative paradigm, mostly used in computer simulations, considers the 'jamming' state. A particle (or a set of particles) is considered jammed if it cannot be translated while fixing the positions of all the other particles in the system [43]. Such a definition was extended by Torquato and Stillinger [28] to different degrees of jamming (local, collective and strict). This approach is very useful in molecular dynamics and other numerical simulations where the system dynamics is involved and the local and collective particle displacements are studied [44]. The conceptual framework associated with this approach is rather similar to the approach used for rigidity, but in this case dynamical properties are considered instead of the static ones. Generally speaking, a rigid state must be a jammed state, but when molecular dynamics simulations are involved, the system is characterized by the state of motion of its elements instead of the static network of forces between elements. In this context the study of the jamming configurations becomes essential for understanding the mechanism which leads to structural arrest. From the perspective of the present study an opposite point of view must be adopted. The question is: starting from the static—jammed—configuration, can we infer the dynamical mechanisms which have produced such a packing? The present paper is an attempt to give some answers in this direction and section 10 specifically addresses this point.

6. Contact network: the topological structure beyond first neighbours

Any force path or any infinitesimal local grain displacement must mechanically propagate from grain to grain through the network of touching grains. The understanding of the hierarchical organization of such a contact network beyond first neighbours is therefore of great importance. Here we apply an approach which was originally developed for the study of crystalline systems [15, 45–49] and disordered foams [50–52]. The topological structure of crystalline frameworks has been intensively studied in terms of the number of atoms that are j bonds away from a given atom [15, 45–49]. If we start from a given 'central' atom, the first 'shell' (distance $j = 1$) is made by all the atoms in contact with the central one. The second shell (distance $j = 2$) is constituted of all atoms which are neighbours to the atoms in the first shell excluding the central one. Moving outward, the atoms at shell $j + 1$ are all the atoms which are bonded to atoms in shell j and which have not been counted previously. In infinite, periodic, crystalline structures with no boundaries, the number of atoms per shell should increase with the topological distance and it has been shown that in several three-dimensional crystalline structures the law of growth for the number of atoms (K_j) at shell j can be given as $K_j = a_j j^2 + b_j j + c_j$ (with a_j, b_j and c_j, coefficients that might vary with j but only within a bounded finite interval) [15, 45–49, 53]. Following the definition of O'Keeffe [48], for these crystalline systems, the asymptotic behaviour of K_j can be characterized in terms of an 'exact topological density': $T_D = \langle a_j \rangle/3$ [53]. It has been noted that such a topological density is interestingly related to the geometrical density of the corresponding crystalline structure and it is a powerful instrument for characterizing such systems. For instance, it is easy to compute that the cubic lattice has $K_j = 4j^2+2$, whereas it has been shown [15] that for Barlow packings of spheres, the K_j are always in a narrow range, within

$$10j^2 + 2 \leqslant K_j \leqslant \left\lfloor \frac{21j^2}{2} \right\rfloor + 2 \qquad (j > 0), \tag{5}$$

with the lower and upper limits corresponding respectively to the fcc (face centred cubic) and hcp (hexagonal close packed) packings. On the other hand, spheres packed in a bcc (body centred cubic) crystalline arrangement have $K_j = 6j^2 + 2$ ($j > 0$).

Beyond perfect crystalline order very few results are known either from theoretical, empirical or numerical points of view. Without much effort one can argue that K_j must grow with a law comparable with the law for a spherical shell: $K_j \sim aj^2 \sim 4\pi j^2$. However, it is also clear that the shape of the growing shell and its roughness can substantially change the coefficient a (as observed in two-dimensional cases [50, 54]). Moreover, it can be shown [55] that in some topological networks the law of growth can follow an intrinsic dimension which is different from the dimension of the embedding space (3 in our case). This mechanism can produce power law growth with exponents different from 2, or different behaviours such as exponential—or even faster—laws of growth [55].

In [9, 10] we reported empirical observations for such a law of growth for disordered packings of nearly equal sized spheres (samples A–F). A precise estimation of the neighbours in contact is quite important also for this kind of measure because this determines the kind of contact network to examine. We observed that the number of spheres at a given topological distance j from a central sphere follows quite accurately a quadratic law: $K_j = aj^2 + c_1 j + c_0$ (see figure 8), with a coefficient a which increases with the threshold δ for the radial distances within which we consider spheres to be connected in the contact network. Such an increment is expected since an enlargement of the threshold distance must correspond to a thickening of the shell. We verify that for threshold distances in the range between $1.02d$ and $1.1d$ a rather linear increment is observed: $a \simeq b\delta + a_0$ (typically with $b \sim \mathrm{O}(1)$). Such a law suggests that the topological density must be associated with the value of the coefficient a at $\delta = 0$: $T_D = a_0/3$. The measured values of the topological densities for all the samples A–F are reported in table 2. They all stay in a rather narrow range around 8.5 and they slightly tend to increase with the sample density. A view of the topological shell structure constructed from a given central sphere in one of the samples is shown in figure 7.

It has been observed by O'Keeffe and Hyde [56] that for *lattice sphere packings* (crystals where the first neighbours are all at the same geometrical distance) a general rule holds: $K_j = (n_\mathrm{c} - 2)j^2 + 2$, giving $T_D = (n_\mathrm{c} - 2)/3$. It is interesting to verify whether this rule is satisfied also for *disordered sphere packings*. In [10, 14] we found that surprisingly for all the disordered packings investigated the topological density is always larger than in the corresponding lattice packing. Such a larger topological density is an indication that the contact network is more compact for disordered systems despite the fact that the *geometrical* density is lower. This fact might have important implications for the system stability and resilience against perturbations and shocks.

So far we have discussed the static structure of the contact network for a given, fixed packing realization. The challenge is to understand its dynamical evolution, its stability and its fragility in response to external actions. Indeed, such a network is extremely sensitive to infinitesimal displacements and it can readjust its structure by means of infinitesimal—zero-energy—moves. The results discussed above indicate that the average properties are related to the sample density. The relevant structural parameter appears to be the topological density which in turn is related to the curvature in the law of growth for the number of grains versus topological distance: $2a = K_{j+1} + K_{j-1} - 2K_j$. Such a curvature (including its fluctuations) is probably the most important control parameter in the contact network. Its relevance was highlighted in two dimensions [50–52] but its study in the three-dimensional case is still to be undertaken.

7. Radial distribution function

The radial distribution function ($g(r)$) is the probability distribution of finding the *centre* of a particle in a given position at distance r from a reference one. This measurement is widely used in geometrical characterization of packing structures and contains information about long range interparticle correlations and their organization [2, 3, 57].

Table 2. Topological densities ($3T_D = a_0$). Most recurrent values for the local orientation order $(\hat{Q}_4, \hat{Q}_6)$. Fraction of local configurations with (Q_4, Q_6) in the range $(\hat{Q}_4 \pm 0.05, \hat{Q}_6 \pm 0.05)$ (dis). Fraction of local configurations close to special forms of order: fcc with (Q_4, Q_6) in the range $(0.191 \pm 0.05, 0.574 \pm 0.05)$; hcp with (Q_4, Q_6) in the range $(0.097 \pm 0.05, 0.485 \pm 0.05)$.

	$3T_D$	r threshold	$(\hat{Q}_4, \hat{Q}_6)$	Disorder (%)	fcc (%)	hcp (%)
A	7.2 ± 0.3					
		1.1	(0.27, 0.47)	23	3	1
		1.2	(0.22, 0.42)	32	2	3
		1.3	(0.18, 0.40)	38	1	5
		1.4	(0.15, 0.36)	42	2	4
B	7.2 ± 0.4					
		1.1	(0.30, 0.45)	24	3	1
		1.2	(0.23, 0.44)	32	2	3
		1.3	(0.16, 0.38)	37	1	5
		1.4	(0.14, 0.35)	43	2	5
C	8.7 ± 0.4					
		1.1	(0.23, 0.46)	28	5	2
		1.2	(0.21, 0.43)	35	3	7
		1.3	(0.15, 0.40)	41	1	11
		1.4	(0.12, 0.37)	45	3	8
D	8.4 ± 0.3					
		1.1	(0.25, 0.44)	28	4	1
		1.2	(0.19, 0.44)	35	2	7
		1.3	(0.15, 0.40)	42	1	11
		1.4	(0.11, 0.36)	46	1	8
E	8.6 ± 0.4					
		1.1	(0.22, 0.44)	27	5	2
		1.2	(0.20, 0.43)	37	3	7
		1.3	(0.15, 0.39)	42	1	12
		1.4	(0.12, 0.36)	47	2	10
F	8.9 ± 0.4					
		1.1	(0.23, 0.44)	31	6	4
		1.2	(0.16, 0.45)	38	4	12
		1.3	(0.13, 0.42)	43	1	17
		1.4	(0.10, 0.38)	47	3	13

In order to measure this quantity one must count the number of sphere centres within a radial distance r from a given one. The average of this number, computed over the whole sample ($n_t(r)$), is related to the radial distribution function by

$$n_t(r_1) - n_t(r_0) = \int_{r_0}^{r_1} g(r) 4\pi r^2 \, dr. \tag{6}$$

Therefore, given the position of the sphere centres, these two quantities $n_t(r)$ and $g(r)$ can be straightforwardly computed. (Some difficulties might arise for small samples, because in this case the spherical shell at distance r from a given sphere might be incomplete and special analytical tools must be used in order to retrieve the correct information [3].) It is easy to compute that the asymptotic behaviour ($r \to \infty$) for the total number of sphere centres inside a spherical region of radius r is $n_t(r) \sim 8\rho(r/d)^3$ ($r \gg d$). Therefore, asymptotically when $r \to \infty$ one expects $g(r) \to 6\rho/(\pi d^3)$. Such a dependence on packing density and bead sizes might turn out to be inconvenient for comparisons between different systems. Therefore,

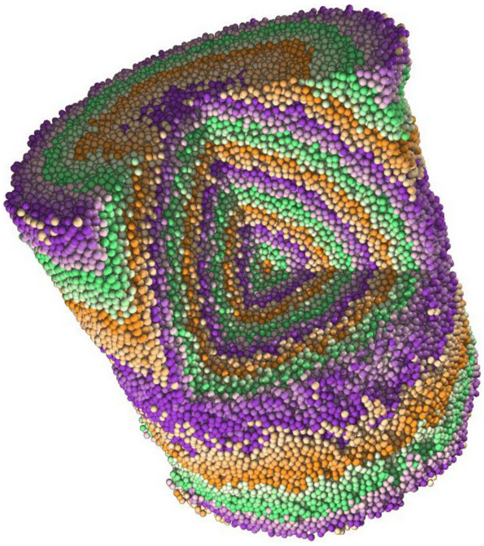

Figure 7. As figure 1 (with a piece removed), but where the topological distances from a given central sphere are highlighted in shades (colours in the online version).

often a *normalized* radial distribution function is used instead:

$$\tilde{g}(r) = \frac{\pi d^3}{6\rho} g(r), \tag{7}$$

which tends to 1 when $r/d \to \infty$.

The first experimental measurement of the radial distribution function in a packing of equal sized spheres was performed by Scott in [2] and subsequently re-analysed by Mason in [3]. They observed a sharp peak at 1.0 diameters (associated with spheres in contact) and a curious 'square' shape of the second peak between 1.7 and 2.0 diameters. After these first observations, unusual enlargements of the second peak and its 'splitting' into two peaks at $r/d \sim \sqrt{3}$ and $r/d \sim 2$ have been generally observed in several experiments and simulations of monosized sphere packings [3, 4, 30, 31, 58]. The presence of peaks after the peak at $r = d$ is a clear indication that the system is organized: a characteristic structure with distinct local patterns is present. To understand which kind of local configuration contributes most to each peak of the $g(r)$ is very important in order to work out which kind of local arrangements generate these globally non-ordered structures. For instance, it is easy to verify that a radial distance $r/d \sim \sqrt{3}$ is consistent with configurations made by placing the centres of four spheres on the vertices of two in-plane equilateral triangles (with edge length d) which share an edge. But it was pointed out in [30] that a large contribution to the peak at $\sqrt{3}$ can also come from configurations made of five spheres placed on the vertices of two tetrahedra which share a common face, whereas the peak at $r/d \sim 2$ is due to three or more spheres which are lying along a (rather) straight line.

Figure 9 shows the normalized radial distribution functions $\tilde{g}(r)$ for the six samples A–F (calculated in [9, 10]). The detail of the close neighbour region (figure 9(*b*)) shows that the two peaks at $r = \sqrt{3}d$ and $r \simeq 2d$ both increase in height with the packing density and—interestingly—the relative growth with the density is faster in the peak at $r = \sqrt{3}d$ with respect to that in the peak at $r \simeq 2d$ (figure 9(*c*)). This certainly indicates an increasing organization in the packing structure but, on the other hand, no signs of crystallization were detected (see section 8).

For all the samples investigated, we found that the behaviour of $\tilde{g}(r)$ at radial distances between $r \simeq 1d$ and $r \simeq 1.4d$ (between the first peak and the first minima) can be quite

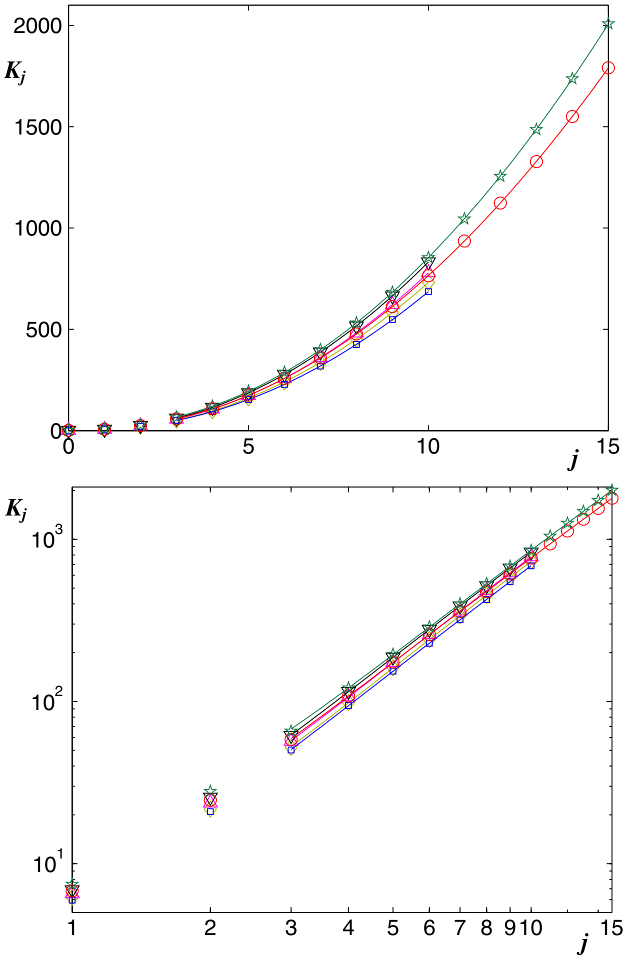

Figure 8. Shell occupation numbers versus topological distances. The symbols indicate the different samples (as in figure 4) and the lines are the best fits using the polynomial form $K_j = a_i j^2 + b_i j + c_i$. These data refer to a threshold distance $1.02d$.

accurately described in terms of a power law singularity:

$$\tilde{g}(r) \sim \frac{c_0}{|r - r_0|^{\alpha}}, \tag{8}$$

with good fits for $r_0 = 1.03d$ and exponents α which increase with the sample density from 0.27 to 0.45 (figure 10(a)). A similar behaviour, but with $\alpha = 0.5$ and $r_0 = d$, was reported in [29] for molecular dynamics simulations. A more recent numerical investigation proposes an exponent $\alpha \sim 0.4$ [59]. In figure 10, we also highlight the growing trend of the exponent α with the density ρ.

Interestingly, the behaviour of $g(r)$ around the other two following peaks (at $r \sim \sqrt{3}d$ and $\sim 2d$) can be described by using similar power law-type divergences. In particular the region $1.4d < r < 1.73d$ is well fitted by the equation (8) with $r_0 = 1.8d$ and exponents α between 0.37 and 0.62, whereas the region $2d < r < 2.15d$ is well fitted by using $r_0 = 2d$ and exponents α between 0.11 and 0.17 (figure 10). We must stress that these are qualitative behaviours: a reliable fit with a power law trend must be performed over several orders of magnitudes on the x and y scales. These linear interpolations on log–log scales must therefore be considered more as indicative behaviours of qualitative laws than fits.

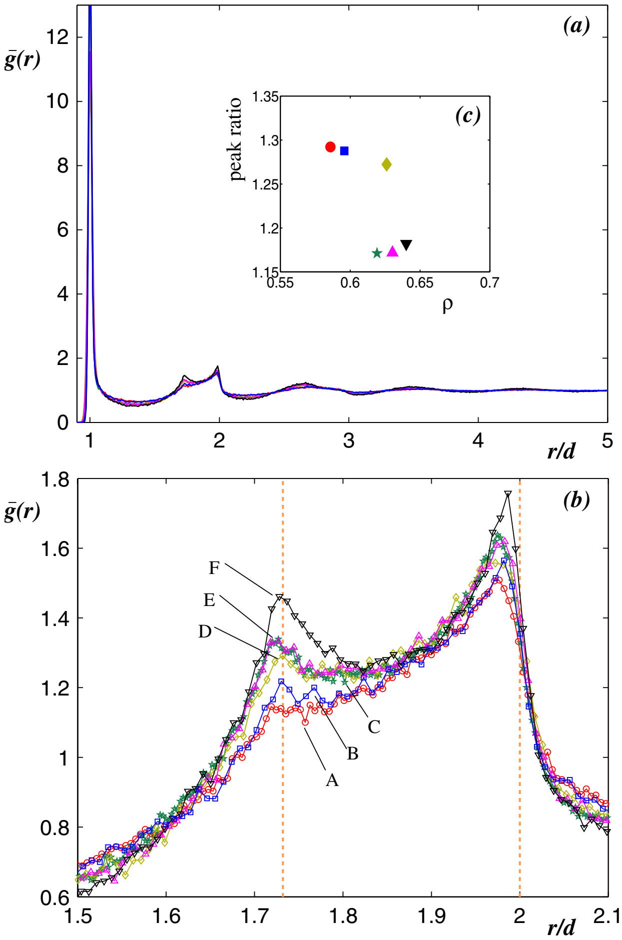

Figure 9. (*a*) Normalized radial distribution function. (*b*) The detail of the two peaks respectively at $\sqrt{2}d$ and $2d$ (vertical lines). (*c*) The ratio between the value of the peak at $2d$ and the peak at $\sqrt{3}d$.

8. Local orientation

We have seen in the previous section that the radial distribution function clearly reveals the existence of a structural organization: some typical lengths (associated with special local configurations) appear repeatedly in the packing. However the fact that there are typical local configurations which repeat often in space does not necessarily imply that there are any long range orders or (poly)crystalline regions. In this section we quantify the kind of local orientational order characteristic of these structures. Revealing and quantifying orientational order is a key issue in establishing the kind of internal organization and in particular determining whether there exists a 'typical' disordered state and identifying possible tendencies towards hidden symmetries. Indeed, if such a 'typical' state exists or/and if there is a tendency toward a specific local organization, then it will be possible to associate with a given granular packing an order parameter which could measure how close the packing is to the 'ideal structure'. On the other hand if one can prove that the system is a collection of uncorrelated local configurations, then this will allow us to calculate the configurational entropy and—consequently—the probability of finding the system in a given state at a given density.

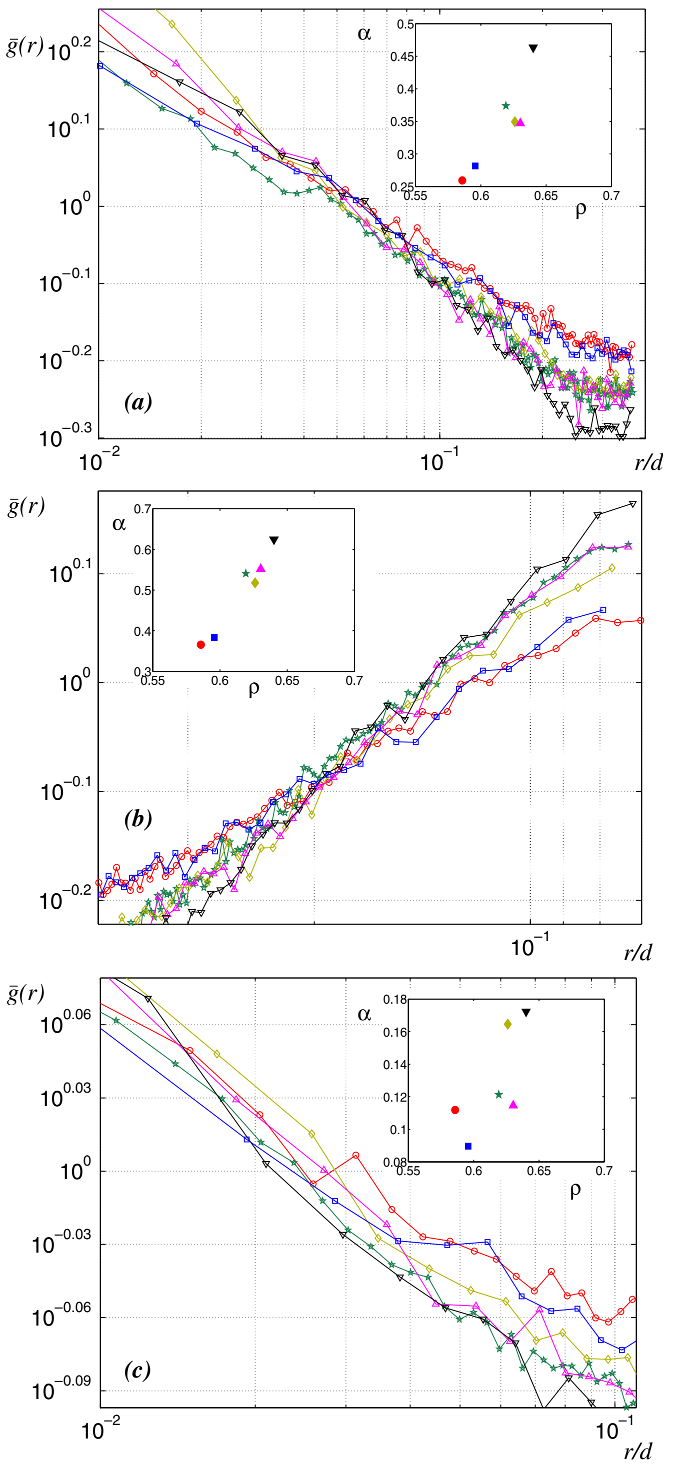

Figure 10. The three peaks of the radial distribution function, respectively (from top to bottom) at $r = 1$, $\sqrt{3}$ and 2, can be described with power law singularities: $g(r) \sim c_0|r - r_0|^{-\alpha}$. The coefficient α depends on the sample densities and their behaviours are reported in the insets.

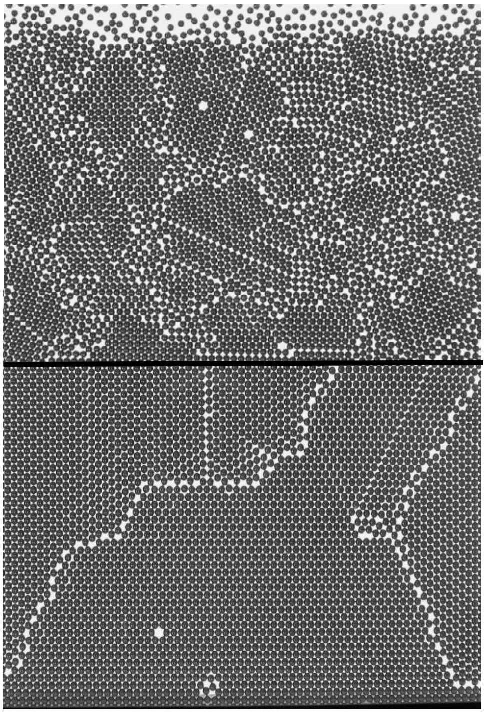

Figure 11. In two dimensions, discs (spheres between two planes in this case) tend to form spontaneously ordered hexagonal patterns which can be combined globally leading to a crystalline order.

Balls under gravity try to minimize the potential energy by choosing a configuration which maximizes the density. It is known that the absolute energy minimum corresponds to an ordered arrangement in stacked planar hexagonal layers forming the so-called Barlow packings [15, 16]. Let us first recall what happens in two dimensions, where it is possible to 'see' the structural arrangement. In two dimensions, when equal discs are poured in a disorderly fashion into a container, they tend to organize themselves locally into close packing configurations but, at first, such a local organization is limited to very short distances yielding an overall disordered assembly (see figure 11, top). Some shaking can increase the density, leading gradually to an overall ordered configuration (figure 11, bottom). It has been argued that a similar mechanism could take place in three dimensions as well. It is however clear from several empirical observations that the tendency toward a crystalline order (even if short ranged) is much less spontaneous in three dimensions than in the two-dimensional case. Such a resilience against becoming ordered has often been associated with 'geometrical frustration', which is present in three dimensions but not in two dimensions. Indeed, in two dimensions six equal discs can be placed touching a given disc forming the densest possible local configuration. Such a configuration is compatible with translational symmetry and it can be repeated infinitely in space leading to a crystalline packing (the triangular lattice). However, in three dimensions the closest possible local configuration is an arrangement of twelve equal spheres touching a central sphere and with centres on the vertices of a regular icosahedron. Such a packing has local density $\rho = 0.754, \ldots$ (which is more than 1% denser than the configurations in Barlow packings at $\rho = 0.740, \ldots$) [16]. But, unlike in the two-dimensional case, such a compact local icosahedral configuration is not compatible with the translational symmetry and therefore it cannot be repeated in space without leaving gaps: it is geometrically frustrated. It has been often argued that the competition between the tendency to form locally compact configurations and the geometrical frustration could be the key to understanding the mechanism of formation of disordered packings and glassy structures. If this is the case, we will expect to see, at the local level, configurations with rotational symmetries characteristic of icosahedral and other close packed structures. The study of the local rotational symmetry can therefore give insights into the mechanism of formation of these structures.

The challenge is to find a measure of rotational symmetry which is invariant with respect to rotations in the system of coordinates. A powerful solution was introduced by Steinhardt *et al* in [27] by assigning a set of spherical harmonics to the vectors $\vec{r}$ between a sphere and its neighbours, $Y_{l,m}(\theta(\vec{r}), \phi(\vec{r}))$ (with $\theta(\vec{r})$ and $\phi(\vec{r})$ the polar and azimuthal angles of $\vec{r}$) and introducing the quantities

$$Q_l = \sqrt{\frac{4\pi}{2l+1}\sum_{m=-l}^{l}|\langle Y_{l,m}(\theta(\vec{r}_i), \phi(\vec{r}_i))\rangle|^2}, \tag{9}$$

with average $\langle(\cdots)\rangle$ over the bonds i in the sample. Such a quantity is invariant under rotations in the coordinate system and it takes characteristic values which can be used to quantify the kind and the degree of rotational symmetry in the system. However, it must be noted that the quantity $Y_{l,m}(\theta(\vec{r}_i), \phi(\vec{r}_i))$ depends on the orientation; therefore in the case of a polycrystalline aggregate, with finite correlation length, its average $\langle Y_{l,m}(\theta(\vec{r}_i), \phi(\vec{r}_i))\rangle$ will decrease and tends to zero with the sample size. To avoid this inconvenience, which makes the comparison between values of Q_l for differently sized samples meaningless, it is convenient to adopt a local measure of Q_l by restricting the average to just over the local bonds between a sphere and its neighbours. In this way, with each sphere in the system can be associated a Q_l and local order can be singled out by counting the number of configurations with Q_l corresponding to special symmetries. In particular the two values of Q_l for $l = 4$ and 6 have special significance. For instance, the simple cubic lattice has $(Q_4, Q_6)^{\mathrm{sc}} = (0.764, 0.354)$, the body centred cubic lattice has $(Q_4, Q_6)^{\mathrm{bcc}} = (0.036, 0.511)$, the fcc one has $(Q_4, Q_6)^{\mathrm{fcc}} = (0.191, 0.574)$, the hcp one has $(Q_4, Q_6)^{\mathrm{hcp}} = (0.097, 0.485)$ and the icosahedral rotational symmetry gives $(Q_4, Q_6)^{\mathrm{ico}} = (0, 0.663)$. Since the lowest non-zero Q_l common to the icosahedral, hexagonal and cubic symmetries is for $l = 6$, it has been argued by several authors that the value of Q_6 is a good indicator of the degree of order in the system and it might be used as an 'order parameter' [43, 58, 60–62]. Indeed, Q_6 is very sensitive to any kind of crystallization and it increases significantly when order appears [60]. An example of the distribution of local (Q_4, Q_6) for the sample C is shown in figure 12 (data from [9, 10]).

Like for the case discussed in the previous sections, in this case the measure depends on the geometrical criteria adopted to identify neighbours. In the literature, several different criteria are used: in [27] all neighbours within $1.2d$ are considered; in [62] the neighbours up to the radial distance which corresponds to the first minima in the radial distribution function ($r \sim 1.4d$; see section 7) were considered; in [60] and [58] the Voronoï (or Delaunay [16, 63]) neighbours were used instead. This last definition might be misleading in some cases (as pointed out by [27]), since the Voronoï method tends to associate bonds also with rather distant neighbours. For instance, an fcc crystalline arrangement (with infinitesimal perturbation) takes two extra neighbours (from 12 to 14 on average) using the Voronoï criteria. Here the influence of the neighbouring criteria is analysed by using four different threshold distances: $\delta = 1.1d$, $1.2d$, $1.3d$ and $1.4d$.

We observe that a very large fraction of local configurations (between 23 and 47%) have local symmetry characterized by (Q_4, Q_6) within a narrow range around their most recurrent

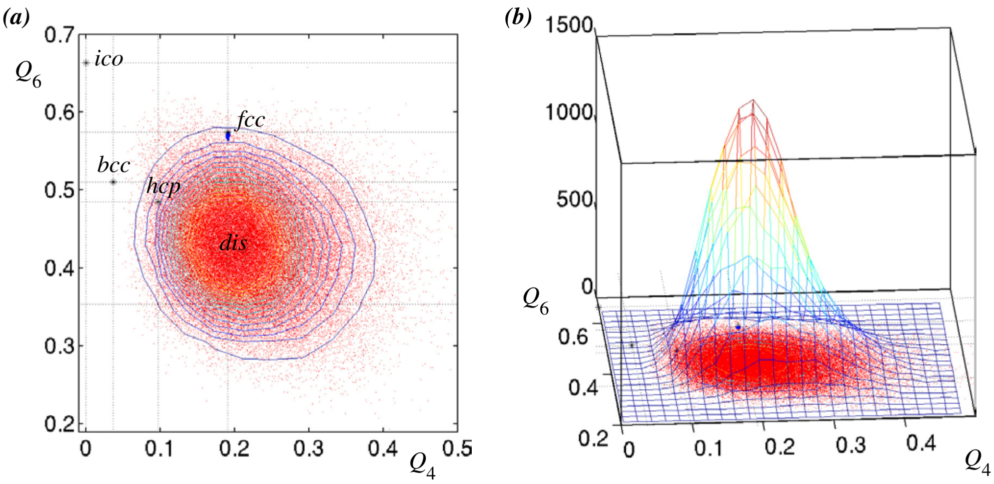

Figure 12. (*a*) The dots are the values (Q_4, Q_6) plotted for all the local configurations in the central region (**G**) of sample C. The lines are contour plots of the frequencies, reported in the 3D plot of (*b*). The positions of specific symmetries in the (Q_4, Q_6) plane are also indicated (ico, bcc, fcc).

values: $(\hat{Q}_4 \pm 0.05, \hat{Q}_6 \pm 0.05)$. The values of $(\hat{Q}_4, \hat{Q}_6)$ range between $0.10 \leqslant \hat{Q}_4 \leqslant 0.30$ and $0.35 \leqslant \hat{Q}_6 \leqslant 0.45$ (see table 2), values which are rather far from any special symmetry. In order to search for signatures of known local symmetries, we measured the fraction of local configurations with (Q_4, Q_6) in a region within a range ± 0.05 from the values in the ideal structures (fcc, hcp, icosahedral, sc and bcc). We found that there are no significant fractions (below 1%) of local configurations with symmetry compatible with icosahedral, simple cubic or bcc; there are a small fraction (between 1 and 6%) of configurations with local symmetry compatible with fcc and there are a fraction of configurations with hcp-type local order which becomes quite significant at large densities (reaching 17% at $\rho = 0.64$ and $\delta = 1.3d$). This occurrence of a rather large fraction of local symmetry with an hcp-like character might suggest the beginning of a crystallization process. However, we have verified that there are no correlations between neighbouring sites with symmetry close to hcp. This excludes the possibility of the presence of any long range hcp order or symmetrical organization beyond first neighbours.

These findings exclude the possibility of the existence of any crystalline order (even at local level) and also cause us to discard the idea that a tendency toward local *frustrated* icosahedral order can be *the* factor responsible for the resilience against crystallization for such packings. On the other hand, these findings, although intriguing, are not conclusive because the origin and nature of the most abundant configurations with $(Q_4, Q_6) \sim (0.25, 0.45)$ are still elusive. In the next section we will try to clarify this point by using different techniques which allow us to view from a different perspective the local packing organization.

9. Geometrical organization around a sphere

The radial distribution function (section 7) clearly shows that despite the fact that these systems are amorphous and disordered, they have a characteristic structural organization which reveals itself with regularities at local level. However, the analysis of the rotational symmetry in the positions of the neighbouring spheres (section 8) does not disclose any known special shape.

In this section we focus on techniques for identifying local correlations which involve more than two neighbouring spheres.

9.1. Voronoï shapes

Let us first consider the analysis of shapes of the Voronoï cells constructed around the centre of each sphere. This is a powerful tool for investigating the local arrangement of spheres and their local organization. The advantage of such a method is that there are no arbitrary choices for the neighbouring criteria. On the other hand, this is also the weakness of the Voronoï method because neighbours which are rather far from the central sphere (typically, up to distances $r/d \sim 1.4$) contribute to the shape of the cell. An extensive analysis was performed by Richard *et al* [60] for hard sphere systems generated by molecular dynamics simulations. They measured the variations of the average number of faces, the standard deviation and the occurrences of faces with four, five and six edges. Interestingly, they found that the shapes of the Voronoï cells have a sharp variation in the region between the freezing and melting point ($0.495 \leqslant \rho \leqslant 0.545$) but—in contrast—there are no notable modifications in their shapes when the system passes from the fluid state to the metastable glassy phase. In this metastable branch they observe that for $0.545 \leqslant \rho \leqslant 0.64$ the average number of faces slightly decreases, whereas the fractions of faces with five or six edges increase and the fraction with four edges decreases. A comparison with the empirical data for bead packings can be made only for this last 'glassy phase' region. In [9, 10] we observed an average number of Voronoï faces which decreases with the density from $\langle f \rangle = 14.6$ at $\rho = 0.586$ (sample A) to $\langle f \rangle = 14.3$ at $\rho = 0.64$ (sample F). This is in very good agreement with simulation results [60], but it clearly shows that this measure has very poor sensitivity to the packing properties. The fractions of faces with four, five and six edges (respectively f_4, f_5 and f_6) follow mixed trends: f_4 decreases from 0.200 to 0.188 (from A to F); f_5 increases from 0.338 to 0.396 (from A to F); f_6 increases from 0.268 to 0.286 (from A to F). Again these values and behaviours are in very good agreement with the ones in [60], but these measures are still too insensitive to the packing properties.

9.2. Common neighbours

An alternative interesting approach called 'common-neighbour analysis of structure' was introduced by Clarke and Jónsson in [30]. They considered two close spheres which stay with centres at a given radial distance and retrieve all the neighbours in common of these two spheres. In general, two touching equal spheres can have a number of common neighbours between 0 and 5. This number is rather sensitive to the local correlations in the packing. Indeed, in [10] we computed the number of common neighbours and in particular the relative occurrence of four and five common neighbours in the six samples A–F. This study revels that the numbers of configurations with four or five common neighbours increase during compaction (see table 3). In particular, when the threshold distance is fixed at $1.1d$, the fraction of edges with four common neighbours (p_4) varies between 17 and 31%, whereas the fraction of configurations with five common neighbours (p_5) grows from less than 3% to above 8% (A to F). This is in agreement with what was observed in computer simulations and suggests that these quantities could be profitably used as 'order' parameters to characterize the packing structure. Indeed, they are much more sensitive than the equivalent quantities obtained from the study of the shape of the Voronoï cell or the Q_4 and Q_6 measurements. But it must be noted that these values depend on the threshold distance used in the neighbouring criteria. However, the overall behaviours and the relative variations are rather steady for a large range of threshold distances between $1.05d$ and $1.15d$.

Table 3. The fraction of configurations with four and five common neighbours and the fraction of configurations with a ring of five bounded common neighbours. The threshold distance is $1.1d$.

	p_4 (%)	p_5 (%)	555 (%)
A	17.5	2.59	0.01
B	18.6	2.66	0.01
C	26.4	6.00	0.06
D	24.4	5.48	0.06
E	26.7	6.11	0.06
F	30.6	8.29	0.09

Clarke and Jónsson [30] describe the local environment in further detail by introducing three indices jkl which specify the local environment of the pair: j is the number of neighbours common to both spheres; k is the number of bonds (linking neighbouring spheres) between the common neighbours; l is the number of bonds in the longest continuous chain formed by the k bonds between the j common neighbours. Different types of pairs are associated with different types of local order. For instance the 555 is a configuration of seven spheres arranged in a close packing typical of icosahedral order. On the other hand, 421 and 422 are characteristic of fcc and hcp order. Computer simulations of hard sphere packing show that during densification (from $\rho = 0.56$ to 0.64) the relative number of 555 and 544 pairs almost double whereas the number of 421 and 422 remain nearly constant suggesting an increase in the local icosahedral order in such systems [30]. However, the results strongly depend on the threshold distance within which two spheres are considered as bonded. It appears therefore worthless to study the local structure in such detail when results are strongly dependent on the assumption for the neighbouring criteria. On the other hand, a very interesting issue in these systems is the possible occurrence of incomplete icosahedral configurations which can be studied by analysing configurations made up of seven spheres arranged in a pentagonal ring around a couple of neighbouring spheres (the '555' configuration). Such a configuration is indeed a 'piece' of an icosahedron and it is therefore a good guide for understanding whether icosahedral configurations play any significant role in the dynamical formation and in the static organization of such structures. But we observe [10] that such configurations are present only in very small fractions (from 0.01 to 0.1%; see table 3), indicating therefore that this kind of close packed local arrangement has very little statistical significance and no relevant physical importance. This observation is in agreement with the results from the (Q_4, Q_6) analysis in section 8 which does not reveal any significant icosahedral symmetry. A further demonstration of this comes from the study of the local volume fractions. In [9, 10] we observe that out of a total number of more than 209 000 local Voronoï configurations only 14 have volume fractions above 0.74 (the fcc one has 0.740, 5 . . . and the icosahedral arrangement has 0.75 . . .). Furthermore, we found that across the samples A–F only 2% of the Delaunay configurations are closed tetrahedra. This reveals that close packed configurations such as the icosahedral one, and also the fcc cell or the regular tetrahedra, play no relevant role in these systems.

9.3. Dihedral angle distribution

A further step toward the understanding of which kinds of local configurations are present in theses systems can be made by analysing the distribution of dihedral angles between common neighbours around a given couple of touching spheres. We have already calculated above the number of common neighbours and shown that the most frequent configurations are the arrangements with four and five common touching spheres. We now study how these spheres

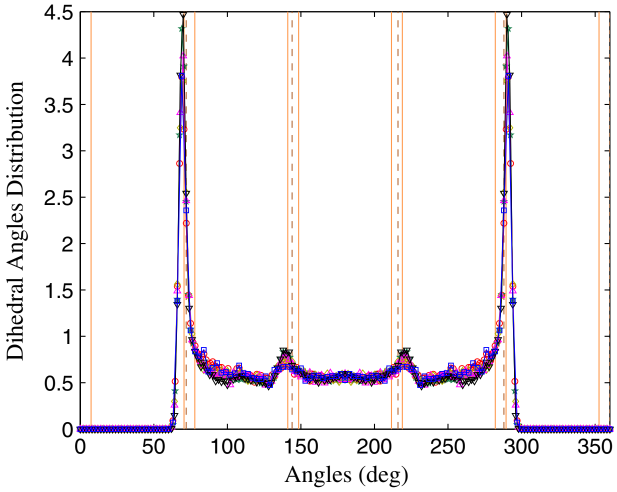

Figure 13. Dihedral angle distribution (x axis: angular degrees; y axis: renormalized frequencies). The vertical lines indicate the angles $\theta = n \arccos(1/3)$ (and $360 - \theta$) with $n = 1, 2, 3, 4, 5$ (tetrahedral packings). The dashed lines are at the angles $\theta = n360/5$ ($n = 1, 2, 3, 4$), which will correspond to icosahedral configurations.

are distributed inside this common ring. In [10] we considered a triangle formed between two spheres in contact and one common neighbour and we measured the dihedral angles between such a triangle and all the other triangles formed with the other common neighbours. The resulting distribution of angles is shown in figure 13. This figure shows a distribution which is symmetric in θ and $360 - \theta$. The largest peak is at $\theta = \arccos(1/3) = 70.5\ldots$ (and $360 - \arccos(1/3) = 289.4\ldots$) which is the dihedral angle in a regular tetrahedron. The smaller peak is at $\theta = 2\arccos(1/3) = 141.0\ldots$ (and $218.9\ldots$) which corresponds to a configuration with two touching tetrahedra. The two peaks for $3\arccos(1/3) = 211.5\ldots$ and $4\arccos(1/3) = 282.1\ldots$ are not clearly visible, being in the same regions as the larger peaks, but a small peak at $5\arccos(1/3) = 352.6\ldots$ (7.356) is visible. This clearly indicates that the common neighbours tend to gather together in the circular ring. Indeed, the case with a uniform angular repartition of common neighbours will lead to a rather different structure of the angular distribution with peaks at $n\pi/3$, $n\pi/4$ and $n\pi/5$, with $n = 1, 2, 3, 4, \ldots$, peaks that are not visible in the empirical distributions in figure 13. It is interesting to note that, similarly to the case for the radial distribution function, the relative heights of the peaks are sensitive to the sample density. But in this case the variations are much less evident than for the $g(r)$.

10. Geometry and structural arrest

In the previous sections we studied the geometrical structure of the disordered sphere packing at rest. Here we try to infer information on the possible dynamical mechanisms which take place during compaction and produce such static structures. The background idea is that the static structure that we are studying empirically is one of several possible inherent states in which the system can be found at the end of its dynamical evolution. Hereafter, when we refer to a dynamics, we imagine a kind of molecular dynamics, where therefore a temperature is well defined and a thermodynamical approach can be used. Following a theoretical approach recently developed [64, 65], we can image the system dynamics, before the structural arrest, developing through configurations which are in the basin of attraction of this final inherent structure. Under this assumption a (thermo)dynamical approach toward this configuration can be reconstructed by performing a virtual, uniform expansion of the system size, reducing in this way the effective density. Such a virtual expansion unjams the spheres allowing them to move in a free volume around the inherent state positions. This is a way to explore the phase space in the basin of attraction associated with the given inherent state. The amount of free space for each sphere will depend on the shape and size of the (expanded) Voronoï cell built around the inherent state configuration. If we consider a uniform expansion by a relative, adimensional, factor h, the volume of the system will change from V to Vh^3. Therefore the factor of expansion is related with the effective density by $h = (\rho^\alpha/\rho)^{1/3}$ (with ρ^α the density of the inherent state α). The volume of each given Voronoï cell v_i around the sphere i will also expand by a factor h becoming: $v_i^\alpha \to v_i^\alpha h^3$. As a consequence of the expansion, the sphere in the cell i will acquire a free volume which can be approximated as $u_i^\alpha = v_i^\alpha (h-1)^3 = v_i^\alpha[(\rho^\alpha/\rho)^{1/3} - 1]^3$. Within a free-volume-like approximation [65] the partition function associated with this basin of attraction is $Q^\alpha = \prod_i u_i^\alpha$. The partition function for the thermodynamic system of spheres is the sum over the contributions from all the inherent states which contribute to such a state:

$$Q = \sum_\alpha \prod_i u_i^\alpha = \sum_\alpha [(\rho^\alpha/\rho)^{1/3} - 1]^{3N} \prod_i v_i^\alpha. \tag{10}$$

The thermodynamical relation $P = k_B T(\partial \ln Q/\partial V)_{N,T}$ can now be used to calculate $\frac{PV}{Nk_B T}$ as a function of the density ρ (the equation of state), yielding for the compressibility factor

$$\frac{PV}{k_B NT} = \sum_\alpha \frac{w^\alpha(\rho)}{1 - (\frac{\rho}{\rho^\alpha})^{1/3}}; \tag{11}$$

with $w^\alpha(\rho)$ the relative weight of the inherent state α at the density ρ: $w^\alpha(\rho) = Q^\alpha/Q$. The calculation of such weights was undertaken in [64, 65] within a 'cell theory' approach, and this will be the topic of a future more detailed paper [66]. Here let us remark that equation (11) predicts a structural arrest at the largest ρ^α when the system is no longer able to sample other denser inherent states. This is what is happening at the maximal compaction ($\rho = 0.74\ldots$) when no denser states are possible. However, a different scenario can be considered: at a certain stage of the compaction the system can be driven into a configuration from which it cannot escape without the use of a very large amount of energy, which in turn implies very long relaxation times. It is therefore dynamically 'trapped' within the basin of attraction of the inherent state α and eventually it will be driven to a structural arrest in a jammed state at $\rho = \rho^\alpha$.

From the analysis of the inherent states A–F, it is possible to understand whether the system is indeed dynamically trapped within these states and therefore to obtain insight into the dynamical process which has led to such a state. In [9, 10] a quantity called the 'escape probability' was calculated. This is the probability that a sphere can move outward from a given local configuration without displacing the positions of its neighbours. Clearly, when such a move is possible, the system can change its geometrical configuration by means of local moves only. This implies that it can dynamically change the basin of attractions and explore the phase space with low energy moves and short relaxation times. In contrast, when the escape probability is zero, a structural rearrangement requires the displacement of a larger number of spheres and the system is more likely to be trapped inside the basin of attraction of this inherent configuration for longer relaxation times. Specifically, in [9, 10] we calculated the gaps between neighbouring spheres and evaluated the size of the largest gap for each local configuration surrounding a given sphere. This quantity is computed by constructing circles through the centres of the Delaunay simplices incident on the central sphere. The central

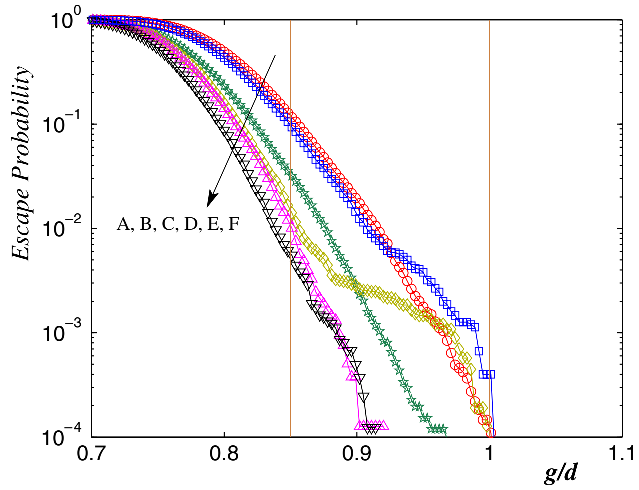

Figure 14. Relative number of configurations with a gap between neighbouring spheres larger than g.

sphere can 'escape' from this configuration only if its diameter (d) is smaller than or equal to the largest radius of such circles. The relative number of local configurations with gaps larger than or equal to a threshold size x is reported in figure 14 for the six samples A–F. We find that all the samples with $\rho > 0.6$ (C–F) have no configuration which allows the central sphere to 'escape', whereas samples A and B have few local configurations with gaps larger than d but seem statistically irrelevant (<0.1%). This strongly suggests that around $\rho \sim 0.58$–0.6 an important phase in the system dynamics reaches an end: above this density, local readjustments involving only the displacement of a single sphere are forbidden. The particle mobility is constrained mostly to within the Voronoï cell and the system compaction can proceed only by involving the collective and correlated readjustment of a larger set of spheres. At this stage the system can no longer sample the whole phase space and it is trapped within the basin of attraction of the inherent state and eventually will reach a structural arrest at $\rho = \rho^{\alpha}$.

For a given density ρ, we can study the system dynamics in the basin of attraction of an inherent state α by virtually expanding the inherent structure by a factor $h = (\rho^{\alpha}/\rho)^{1/3}$ ($\rho \leqslant \rho^{\alpha}$). Within the selected basin of attraction the sizes of the gaps between neighbouring cells scale with the expansion factor h plus a quantity $(h-1)d$ which is the available space in which the spheres can freely displace around the average position ($h > 1$). From the distribution of maximal gaps between neighbouring spheres at the inherent state ($h = 1$) we can therefore retrieve the distribution of maximal gaps when the system has been expanded by any factor h. The escape probability associated with a system in the basin of attraction of the inherent state α is given by the relative number of local configurations with maximal gaps larger than d at a given h. This corresponds to the relative number of inherent configurations with maximal gaps larger than $(2-h)d/h$. Applying this criterion to the fcc crystalline arrangement one can calculate that a system in the basin of attraction of the inherent state associated with this crystalline packing becomes trapped with an escape probability equal to zero for densities larger than $\pi\sqrt{18}(2+\sqrt{3})^3/64 = 0.6014\ldots$. The same criterion can be applied to the inherent structures A–F to obtain the density ρ at which such finite systems become trapped. In figure 15 the escape probabilities (the number of local configurations with gaps larger than

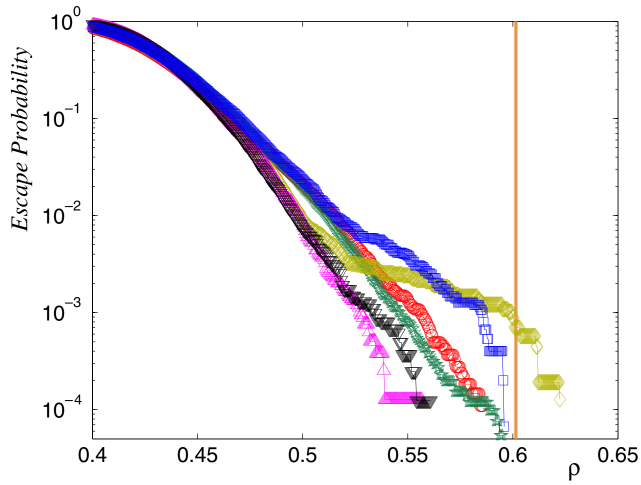

Figure 15. Escape probability versus density for systems in the basin of attraction of the inherent states A–F. The vertical line indicates the density above which the escape probability becomes zero in the fcc packing.

$(2-h)d/h$ divided by the total number of local configurations) for the six samples A–F at various expansions h are reported as a function of the sample 'virtual' densities ($\rho = \rho^{\alpha}/h^3$). We observe that all the samples have escape probabilities which decrease fast with the density and they have become smaller than 10^{-2} already for densities around 0.5. The probabilities continue to decrease between densities 0.5 and 0.55 where they become zero for samples E and F. On the other hand for samples A, B, C the probabilities go to zero around 0.6. Sample D shows a different behaviour, becoming zero above 0.6, but this is likely to be caused by a defect in the sample. Indeed, the number of configurations in the sample is 1.5×10^4, which means that probabilities below 10^{-3} refer to only a few open configurations in the sample.

In principle, a complete study of the system densification dynamics requires information about *all* the accessible inherent states and their relative weights. This clearly goes beyond the scope of the present paper and it will be the topic of following works. However, let me note that the results strongly suggest that for densities below ~0.6 the system can still explore the configuration space and a sufficiently slow cooling dynamics should take the system to crystallization. On the other hand, beyond the density $\pi\sqrt{18}(2+\sqrt{3})^3/64 = 0.6014\ldots$, the system is trapped in the basin of attraction of the reference packing (crystalline or disordered). Therefore if the system is compressed above 0.601, in a way which avoids the crystalline branch, then any cooling dynamics will drive it to a structural arrest in a disordered jammed configuration.

11. Conclusions

The granular organization at local level was first studied by analysing the fluctuations of the local volumes (section 3) associated with two ways of subdividing the volume into local parts: the Delaunay and the Voronoï partitions. It has been pointed out that the local volumes have skewed distributions with power law tails for the large volumes. By following Edwards [22–24] this should allow one to retrieve the 'granular compactivity'. However, it has been shown that Delaunay and Voronoï volumes follow rather different distributions, posing serious questions as regards which kind of space partition is appropriate in these studies. The local topology at grain level has been studied in section 4 where a clear dependence between the number of neighbours and the sample density has been pointed out. It has been discussed that this might suggest a scenario where a rigid percolation takes place around $\rho = 0.55$ where the average number of contacts per sphere is $n_c = 4$. The study of the local rotational symmetry (section 8) shows that a very large fraction of the local configurations are in a region of (Q_4, Q_6) around the values (0.25, 0.45) which is distinct from any known symmetry. This, together with the analysis of local volume fractions and correlations, excludes the possibility of the existence of any partial crystallization in the samples and also excludes the possibility of any relevant icosahedral order in the packing. The distributions of the dihedral angles (section 9) indicate that a typical local configuration is made up of four or five spheres which tend to gather together in a compact portion of a ring around a common pair of neighbours. The hierarchical structure has been investigated both geometrically (section 7) and topologically (section 6); the indication is that these systems are disordered but not random and a characteristic organization, which depends on the sample density, is present both at local and global level. We pointed out that the topological density in disordered sphere packings is always larger than the topological density in the corresponding lattice sphere packings. Such a larger topological density is an indication that the contact network is more compact in disordered systems despite the fact that the *geometrical* density is lower. This might have important implications for the system stability and resilience against perturbations and shocks. The dynamics toward structural arrest has been analysed in section 10 where it has been pointed out that above the density 0.601 movement of a sphere away from its local environment is no longer possible without displacing the first neighbours. It has been commented that this implies a dynamical trapping of the system in the basin of attraction of the relative inherent state leading to a structural arrest.

Acknowledgments

Many thanks to T J Senden, M Saadatfar, A Sakellariou for several discussions and the tomographic data. I am grateful to A Limaye for the volume rendered images. This work was partially supported by the ARC discovery project DP0450292 and Australian Partnership for Advanced Computing National Facilities (APAC).

References

[1] Bernal J D and Mason J 1960 *Nature* **188** 910
[2] Scott G D 1962 *Nature* **194** 956
[3] Mason G 1968 *Nature* **217** 733
[4] Seidler G T, Martinez G, Seeley L H, Kim K H, Behne E A, Zaranek S, Chapman B D, Heald S M and Brewe D L 2000 *Phys. Rev.* E **62** 8175
[5] Sederman A, Alexander P and Gladden L F 2001 *Powder Technol.* **117** 255
[6] Richard P, Philippe P, Barbe F, Bourlès S, Thibault X and Bideau D 2003 *Phys. Rev.* E **68** 020301
[7] Brujić J, Edwards S F, Hopkingson I and Makse H A 2003 *Physica* A **327** 201
[8] Kohonen M M, Geromichalos D, Scheel M, Schier C and Herminghaus S 2004 *Physica* A **339** 7
[9] Aste T, Saadatfar M, Sakellariou A and Senden T J 2004 *Physica* A **339** 16
[10] Aste T, Saadatfar M and Senden T J 2005 *Phys. Rev.* E at press
(Aste T, Saadatfar M and Senden T J 2005 *Preprint* cond-mat/0502016)
[11] Sakellariou A, Sawkins T J, Senden T J and Limaye A 2004 *Physica* A **339** 152
[12] Sheppard A, Sok R and Averdunk H 2004 *Physica* A **339** 145
[13] Aste T and Senden T J 2005 in preparation
[14] Aste T and Senden T J 2005 *Proc. Powders Grains* 2005
[15] Conway J and Sloane N 1997 *Proc. R. Soc.* A **453** 2369
[16] Aste T and Weaire D 2000 *The Pursuit of Perfect Packing* (Bristol: Institute of Physics Publishing)
[17] Knight J B, Fandrich C G, Lau C N, Jeager H M and Nagel S R 1995 *Phys. Rev.* E **51** 3957

[18] Nowak E R, Knight J B, Povinelli M L, Jeager H M and Nagel S R 1997 *Powder Technol.* **94** 79
[19] Nowak E R, Knight J B, BenNaim E, Jeager H M and Nagel S R 1998 *Phys. Rev.* E **57** 1971
[20] Philippe P and Bideau D 2002 *Europhys. Lett.* **60** 677
[21] Onoda G Y and Liniger E G 1990 *Phys. Rev. Lett.* **64** 2727
[22] Edwards S and Oakeshott R 1989 *Physica* A **157** 1080
[23] Edwards S 1994 *Granular Matter: An Interdisciplinary Approach* (New York: Springer) pp 121–40
[24] Edwards S F, Brujić J and Maskse H A 2004 *A Basis for the Statistical Mechanics of Granular Systems* (Amsterdam: Elsevier)
[25] Smith W O, Foote P D and Busang P F 1929 *Phys. Rev.* **34** 1271
[26] Mason G and Clark W 1966 *Nature* **211** 957
[27] Steinhardt P J, Nelson D R and Ronchetti M 1983 *Phys. Rev.* B **28** 784
[28] Torquato S and Stillinger F 2001 *J. Phys. Chem.* B **29** 11849
[29] Silbert L E, Ertas D, Grest G S, Halsey T C and Levine D 2002 *Phys. Rev.* E **65** 031304
[30] Clarke A S and Jónsson H 1993 **47** 3975
[31] Yang R Y, Zou R P and Yu A B 2000 *Phys. Rev.* E **62** 3900
[32] Hill T 1956 *Statistical Mechanics* (New York: McGraw-Hill)
[33] Lagrange J 1788 *Mécanique Analytique* Paris
[34] Maxwell J C 1864 *Phil. Mag.* **27** 294
[35] Edwards S F and Grinev D V 1999 *Phys. Rev. Lett.* **82** 5397
[36] Micoulaut M 2002 *Europhys. Lett.* **58** 330
[37] Moukarzel C 1996 *J. Phys. A: Math. Gen.* **29** 8079
[38] Graver J E 2001 *Counting on Frameworks* vol 25 (Washington: The Mathematical Association of America, Dolciani Mathematical Expositions)
[39] Thorpe M F and Chubynsky M V 2001 *Rigidity and Self-Organization of Network Glasses and the Intermediate Phase* (Dordrecht: Kluwer–Academic)
[40] Moukarzel C F 1998 *Phys. Rev. Lett.* **81** 1634
[41] Chubynsky M V and Thorpe M F 2001 *Curr. Opin. Solid State Mater. Sci.* **5** 525
[42] Ball R C and Blumenfeld R 2002 *Phys. Rev. Lett.* **88** 115505
[43] Torquato S, Truskett T M and Debenedetti P G 2000 *Phys. Rev. Lett.* **84** 2064
[44] Donev A, Torquato S, Stillinger F H and Connelly R 2004 *J. Appl. Phys.* **95** 989
[45] Brunner G O and Laves F 1971 *Wiss. Z. Techn. Univ. Dresd.* **20** 387
[46] Brunner G O 1979 *J. Solid State Chem.* **29** 41
[47] O'Keeffe M 1991 *Acta Crystallogr.* A **47** 748
[48] O'Keeffe M 1991 *Z. Kristallogr.* **196** 21
[49] O'Keeffe M 1995 *Z. Kristallogr.* **210** 905
[50] Aste T, Szeto K Y and Tam W Y 1996 *Phys. Rev.* E **54** 5482
[51] Aste T, Boosé D and Rivier N 1996 *Phys. Rev.* E **53** 6181
[52] Aste T 1999 *Foams and Emulsions* ed J F Sadoc and N Rivier (Amsterdam: Kluwer) pp 497–510
[53] Grosse-Kunstleve R W, Brunner G O and Sloane N J A 1996 *Acta Crystallogr.* A **52** 879
[54] Ohlenbusch H, Aste T, Dubertret B and Rivier N 1998 *Eur. Phys. J.* B **29** 211
[55] Aste T, Di Matteo T and Hyde S T 2005 *Physica* A **346** 20 (*Preprint* cond-mat 0408443)
[56] O'Keeffe M and Hyde B G 1996 *Crystal Structures, Patterns and Symmetry* vol 1 (Washington, DC: Mineralogical Society of America)
[57] Bideau D and Hansen A (ed) 1993 *Disordered and Granular Media* (Amsterdam: North-Holland)
[58] Kansal A R, Torquato S and Stillinger F H 2002 *Phys. Rev.* E **66** 041109
[59] Donev A, Torquato S, Stillinger F H and Connelly R 2004 *Preprint* cond-mat/0408550
[60] Richard P, Oger L, Troadec J-P and Gervois A 1999 *Phys. Rev.* E **60** 4551
[61] Richard P, Oger L, Troadec J-P and Gervois A 1999 *Europhys. Lett.* **48** 415
[62] Truskett T M, Torquato S and Debnedetti P G 2000 *Phys. Rev.* E **62** 993
[63] Voronoï G 1908 *J. R. Angew. Math.* **134** 198
[64] Aste T and Coniglio A 2003 *J. Phys.: Condens. Matter* **15** S803
[65] Aste T and Coniglio A 2004 *Europhys. Lett.* **67** 165
[66] Aste T and Coniglio A 2004 in preparation